

# Electric field-driven coherent spin reorientation of optically generated electron spin packets in InGaAs

S. Kuhlen,<sup>1,2</sup> K. Schmalbuch,<sup>1,2</sup> M. Hagedorn,<sup>1,2</sup> P. Schlamme,<sup>1,2</sup>  
M. Patt,<sup>1,2</sup> M. Lepsa,<sup>3,2</sup> G. Güntherodt,<sup>1,2</sup> and B. Beschoten<sup>1,2,\*</sup>

<sup>1</sup>*II. Physikalisches Institut, RWTH Aachen University, 52056 Aachen, Germany*

<sup>2</sup>*JARA-Fundamentals of Future Information Technology,  
Jülich-Aachen Research Alliance, Germany*

<sup>3</sup>*Peter Grünberg Institut (PGI-9), Forschungszentrum  
Jülich GmbH, D-52425 Jülich, Germany*

(Dated: July 22, 2011)

## Abstract

Full electric-field control of spin orientations is one of the key tasks in semiconductor spintronics. We demonstrate that electric field pulses can be utilized for phase-coherent  $2\pi$  spin rotation of optically generated electron spin packets in InGaAs epilayers using time-resolved Faraday rotation. Through spin-orbit interaction, the electric-field pulses act as local magnetic field pulses (LMFP). Their field strength is determined by Hanle depolarization measurements. By the temporal control of the LMFP, we can turn on and off electron spin precession and thereby rotate the spin direction into arbitrary orientations in a 2-dimensional plane.

Most device concepts in semiconductor spintronics rely on the efficient generation of spin-polarized carriers and their phase sensitive manipulation and read-out. Initial experiments comprised ferromagnet/semiconductor hybrid structures, where the ferromagnet is either used as a source of spin-polarized carriers [1–3] or as a spin-sensitive detector using magnetoresistive read-out [4]. In recent years, however, a new pathway towards spintronics without ferromagnets has evolved, which allows to generate and to manipulate spins by electric fields only [5]. In ordinary non-magnetic semiconductors, dc electric fields can generate spins by two complementary effects, the spin Hall effect [6–11] and the so-called current induced spin polarization (CISP) [12–15]. Both result from the spin-orbit (SO) coupling. The spin Hall effect leads to a spin accumulation transverse to the current flow direction by spin dependent scattering [8], while CISP is manifested by a uniform spin polarization in the semiconductor, which has been proven both by static and by time-resolved magneto-optical probes [13]. Although the microscopic origin of CISP is not fully understood [12, 16–18], in most systems electron spins get oriented along the effective internal magnetic field, which can be tuned by the electric field strength through SO coupling. Internal magnetic fields have also been determined in 2D electron gases by Shubnikov-de Haas oscillations [19, 20], antilocalization [21], photo-current [22], and time-resolved Faraday rotation (TRFR) measurements [23, 24]. The control of the internal fields is of fundamental importance for spin manipulation. It can be realized by gate voltages in 2D electron gases [25] or by dc electric fields [26, 27]. These SO fields have also been used to induce spin precession at zero external magnetic field [27].

In this Letter we report on time-resolved electrical spin manipulation experiments of electron spins in InGaAs. Coherent spin packets are optically generated by circularly polarized laser pump pulses. Their initial direction is manipulated by electrical field pulses, which act as effective internal magnetic field pulses due to SO coupling. Using TRFR we probe the Larmor precession induced by the SO field pulse. By changing the pulse width we are able to rotate the spins into arbitrary directions within a 2-dimensional plane.

Our studies were performed on a 500 nm thick  $\text{In}_{0.07}\text{Ga}_{0.93}\text{As}$  epilayer grown on semi-insulating (100) GaAs by molecular beam epitaxy. The room temperature carrier density was set to  $n \sim 3 \times 10^{16} \text{ cm}^{-3}$  by Si-doping to allow for long spin dephasing times at low temperatures [28, 29]. By chemical wet etching a 160  $\mu\text{m}$  wide and 200  $\mu\text{m}$  long transport channel was patterned and contacted with standard Au/Ge/Ni electrodes. For spin manipulation experiments, the electric field was applied along the  $[01\bar{1}]$  crystal axis as shown in

Fig. 1a. For our samples, this configuration yields the strongest CISP with internal magnetic fields pointing along the [011] or  $y$  axis (see also [13]). The device is embedded in a coplanar wave guide and connected to microwave probes. In the following, we discuss two classes of experiments: (I) In static CISP, we will use dc  $E$  fields to probe the  $E$  field induced spin polarization measuring the Faraday rotation  $\theta_F$  in polar geometry (along the [100] or  $z$  axis). From the shape of the resulting Hanle depolarization curves we are able to directly extract the internal magnetic field strength  $\vec{B}_{int}$  at non-collinear alignment of  $\vec{B}_{int}$  and the external magnetic field  $\vec{B}_{ext}$  (see Fig. 1a). (II) In experiments on TRFR, we use circularly polarized ps laser pump pulses to trigger electron spin coherence in InGaAs. Spin precession about the vector sum of  $\vec{B}_{int}$  and  $\vec{B}_{ext}$  is probed by a second time-delayed linearly polarized probe pulse using standard measurements of  $\theta_F$ .  $\vec{B}_{int}$  can either result from dc or pulsed electric fields. The latter stems from a pulse-pattern generator, which is temporally synchronized to the picosecond laser and is used for time-resolved spin reorientation experiments.

We first use dc-CISP to determine the internal magnetic field direction and its magnitude in our InGaAs structures. Fig. 1b shows the magnetic field dependent  $\theta_F$  signal taken at  $T = 30$  K and  $E_{dc} = +5 \frac{\text{mV}}{\mu\text{m}}$  for  $\vec{B}_{ext}$  applied along the  $x$  direction ( $\alpha = 90^\circ$ ). As expected, we observe  $\theta_F = 0$  at  $\vec{B}_{ext} = 0$  proving the in-plane orientation of the spin polarization. At  $\vec{B}_{ext} \neq 0$ , spins start to precess into the perpendicular observation direction, which is given by the probe beam direction. The sign of  $\theta_F$  changes with the sign of  $B_{ext}$ , as the spins precess into opposite directions, i.e. into the  $\pm z$  direction. The resulting antisymmetric Hanle depolarization curve clearly demonstrates that the spin polarization  $S_0$  is oriented along the  $y$  direction, i.e. parallel to  $\vec{B}_{int}$ .

Assuming  $\vec{B}_{int} \perp z$  and an initial spin orientation  $S_0 \parallel \vec{B}_{int}$ , we can model [30] the Hanle curves by

$$\theta_F(B_{ext}) = \theta_0 \cdot \frac{B_{ext} \cdot \sin \alpha}{B_{1/2}} \cdot \left[ 1 + \left( \frac{B_{tot}}{B_{1/2}} \right)^2 \right]^{-1}, \quad (1)$$

with amplitude  $\theta_0 \propto S_0$ , and the total effective magnetic field  $\vec{B}_{tot}(B_{int}, B_{ext}, \alpha) = \vec{B}_{int} + \vec{B}_{ext}$ . The width of the Hanle curve  $B_{1/2}$  is a direct measure of the transverse spin dephasing time  $T_2^* = (\gamma B_{1/2})^{-1}$ , with  $\gamma$  being the gyromagnetic ratio. As seen from Fig. 1c, we observe a strong decrease of  $T_2^*$  for both  $E$  field polarities, which has also been observed in Ref.[13] indicating additional  $E$  field dependent spin dephasing.

We now apply  $\vec{B}_{ext}$  along  $\vec{B}_{int}$  at  $\alpha = 0^\circ$ . In this geometry  $\theta_F$  vanishes at all magnetic

fields (see Fig. 2a) confirming that the spin orientation is parallel to  $\vec{B}_{ext}$ . When changing  $\alpha$  from 0 to  $90^\circ$ , we expect a continuous increase of the precession angle and thus of the  $z$  component of the observable spin vector. Fig. 2b shows the Hanle curve measured at  $\alpha = 45^\circ$ . The most striking difference to the antisymmetric Hanle curve shown in Fig. 1b for  $\alpha = 90^\circ$  is the different amplitude of  $|\theta_F|$  at its extremal values (see arrows in Fig. 2b), which varies, e.g., in Fig. 2b by a factor of three. Such asymmetric Hanle curves have not been reported so far. However, they are straightforward to be explained if we consider spin precession about  $\vec{B}_{tot}$ . As illustrated in the upper panel of Fig. 2b for  $\alpha = 45^\circ$ , the respective magnitude of  $\vec{B}_{tot}$  differs for  $\pm \vec{B}_{ext}$ . Additionally, the angle between  $\vec{B}_{tot}$  and  $\vec{S}_0$  changes significantly. For  $E = +5 \frac{\text{mV}}{\mu\text{m}}$ , the largest precession angle is achieved for negative  $B_{ext}$ , when  $\vec{B}_{tot} \perp \vec{B}_{int}$ . For positive  $B_{ext}$ , however, the precession angle gets significantly reduced resulting in smaller  $\theta_F$  values, which explains the observed asymmetry. As shown in

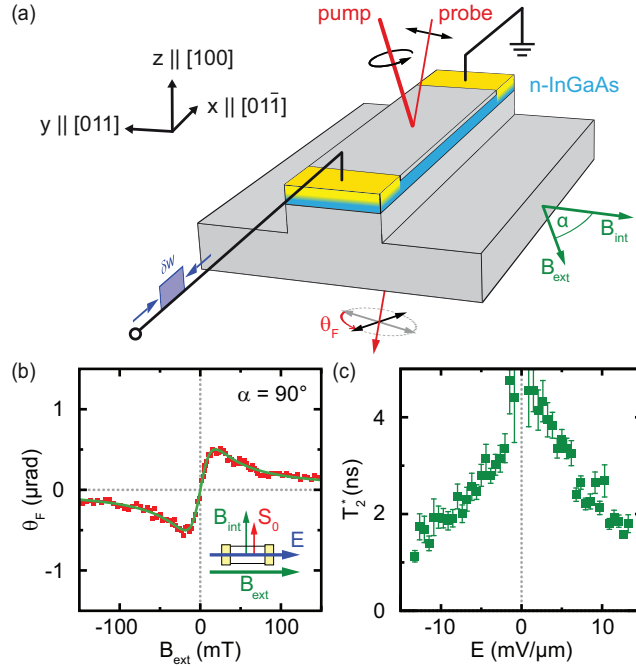


Figure 1: (color online). (a) Schematic setup for dc CISP and coherent spin manipulation experiments. DC or pulsed  $E$  fields are applied along the  $[0\bar{1}\bar{1}]$  direction of an  $n$ -InGaAs transport channel. Electrically or optically generated spins are probed by static and TRFR in polar geometry.  $\vec{B}_{ext}$  deviates from  $\vec{B}_{int}$  by the angle  $\alpha$ . (b) Antisymmetric Hanle depolarization curve taken at  $\alpha = 90^\circ$ ,  $E = +5 \frac{\text{mV}}{\mu\text{m}}$  and  $T = 30$  K. The green line is a fit according to Eq. 1. (c) Spin dephasing time  $T_2^*$  as a function of dc  $E$  field.

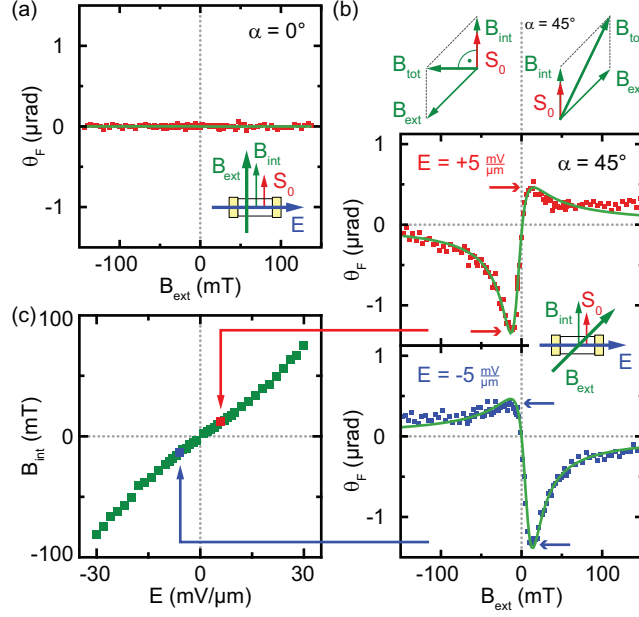


Figure 2: (color online). Hanle measurements under different angles  $\alpha$  between  $\vec{B}_{int}$  and  $\vec{B}_{ext}$  ( $T = 30$  K). (a) No Hanle signal is observed at  $\alpha = 0^\circ$  showing that spins are oriented parallel to  $\vec{B}_{ext}$  (b) (upper panel) Schematic sketch for the total effective magnetic field  $\vec{B}_{tot}$  ( $\alpha = +45^\circ$ ) being the vector sum of  $\vec{B}_{int}$  and  $\vec{B}_{ext}$  for positive and negative  $B_{ext}$ . (lower panel) Hanle measurements for  $\alpha = 45^\circ$  taken at  $E = \pm 5 \frac{\text{mV}}{\mu\text{m}}$  and  $T = 30$  K. The striking asymmetry of the Hanle curve between positive and negative  $B_{ext}$  stems from the concurrent change of  $\vec{B}_{tot}$ . A reversal of  $E$  reverses  $B_{int}$  and the spin signal. The green lines are fits to Eq. 1. (c)  $B_{int}$  vs. dc  $E$  field determined by fitting the asymmetric Hanle signal.

Fig. 2b (lower panel), a sign reversal of the  $E$  field leads to both a sign reversal of the Hanle curve and a mirroring of the asymmetric deformation. Both result from a sign reversal of  $\vec{B}_{int}$  and  $\vec{S}_0$ . The Hanle curves can be fitted according to Eq. 1 (see green curves in Fig. 2b). The extracted  $B_{int}$  values in Fig. 2c vary almost linearly with the  $E$  field and vanish at  $E = 0$  (see also [23]). Large  $B_{int}$  values of  $\pm 80$  mT are obtained at moderate  $E$  fields, which will be used next for coherent spin manipulation experiments.

For this purpose, coherent spins are generated by laser pump pulses and detected by a conventional TRFR setup in polar geometry. By absorption of circularly polarized picosecond laser pulses, coherent electron spin ensembles are generated along the out-of-plane  $z$  direction [29, 31]. The electric field will now be used for spin manipulation only. We note that the  $E$  field pulse itself can also create a phase triggered coherent spin polariza-

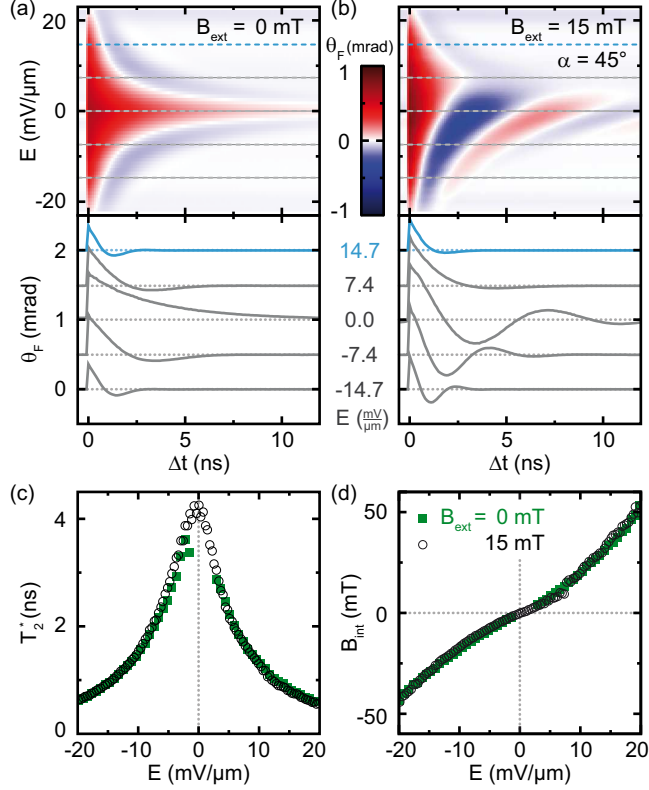


Figure 3: (color online). TRFR after optical spin orientation in InGaAs ( $T = 30$  K). Electron drift in an  $E$  field induces  $B_{int}$  which results in spin precession about  $\vec{B}_{tot} = \vec{B}_{int} + \vec{B}_{ext}$ , shown for (a)  $B_{ext} = 0$  mT and (b)  $B_{ext} = 15$  mT at  $\alpha = 45^\circ$ . TRFR scans are plotted in the lower parts at selected  $E$  fields. An offset is added for clarity. The resulting parameters (c)  $T_2^*$  and (d)  $B_{int}$  are in good agreement with the values extracted from Hanle measurements (Figs. 1c and 2c).

tion, which can be probed by time-resolved CISP [13]. This effect is, however, negligible as the fraction of spin polarization by CISP is three orders of magnitude less than the spin polarization obtained after optical orientation.

We first explore the influence of static dc  $E$  fields on the coherent spin ensemble in Figs. 3a and b at  $\vec{B}_{ext} = 0$  mT and 15 mT, respectively. From these experiments it is obvious that SO induced electron spin precession can be triggered by electrical means. In the former case, for both negative and positive  $E$  fields of the same magnitude the spins precess with equal Larmor frequencies  $\omega_L = g \frac{\mu_B}{\hbar} B_{tot}$ , where  $g$  is the electron g-factor,  $\mu_B$  Bohr's magneton, and  $\hbar$  Planck's constant. In contrast, spin precession is accelerated in the latter case (see Fig. 3b) for  $E < 0 \frac{\text{mV}}{\mu\text{m}}$  while it is slowed down for  $0 < E < 7.5 \frac{\text{mV}}{\mu\text{m}}$ . This dependence proves

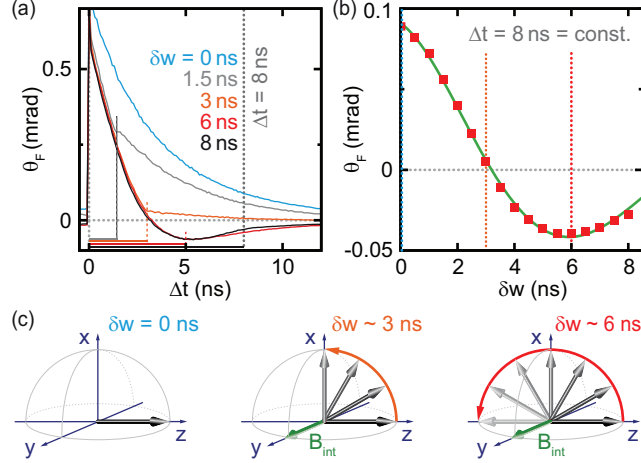


Figure 4: (color online). (a) TRFR measurements of optically created spin packets ( $T = 30$  K), which precess in a local magnetic field pulse arising from  $E$  field pulses of different width  $\delta w$ . All  $E$  field pulses start at  $\Delta t = 0$  ns. After the pulses have stopped, spins decay with the intrinsic spin dephasing time at  $B = 0$ . (b)  $\theta_F$  at  $\Delta t = 8$  ns (dotted line in Fig. 4a) vs pulse widths  $\delta w$ . The solid line is a fit to the data (see text for details). (c) Illustration of coherent spin rotation. Spins are created along the  $+z$  direction. For a  $\pi/2$  pulse ( $\delta w \sim 3$  ns) spin precession stops along the  $+x$  direction while for a  $\pi$  pulse ( $\delta w \sim 6$  ns) spins rotate into the  $-z$  direction.

the reversal of the internal magnetic field direction upon sign reversal of the  $E$  field. For  $E = 0 \frac{\text{mV}}{\mu\text{m}}$  multiple spin precessions can be observed due to the enhanced  $T_2^*$ .

All TRFR data can be described by an exponentially damped cosine function

$$\theta_F(\Delta t) = \theta_0 \cdot \exp\left(-\frac{\Delta t}{T_2^*}\right) \cdot \cos(\omega_L \Delta t + \delta), \quad (2)$$

with amplitude  $\theta_0$ , pump-probe delay  $\Delta t$  and an additional phase factor  $\delta$ . This way we can determine  $T_2^*$  and  $B_{int}$ , which are shown in Figs. 3c and d, respectively, as function of  $E$ . We note a strong decrease of  $T_2^*$ , which limits the observable spin coherence. The decrease of  $T_2^*$  has previously been assigned to spins drifting out of the probe laser focus [27]. However, as the dephasing times extracted from the above CISP measurements (cp. to Fig. 1c) exhibits a similar decrease with  $E$  field, we attribute this effect to additional spin dephasing, which is caused by the  $E$  field induced internal magnetic fields. As in CISP (see Fig. 2c),  $B_{int}$  values from TRFR depend also nearly linearly on the  $E$  field.

While in the above dc experiments we can control the spin precession frequency by electric fields only, we now want to manipulate the phase of the optically generated coherent spin

packet. In other words, we will use  $E$  field pulses both to initialize and to stop spin precession at  $B_{ext} = 0$  mT. When the  $E$  field pulse reaches the optically generated spin packet, it will create a LMFP for the duration of the pulse. This LMFP will trigger spin precession in the  $zx$ -plane (see Fig. 1a). The precession frequency depends on the  $E$  field strength, while the total precession time is given by the pulse width  $\delta w$ . In Fig. 4a we show a sequence of TRFR measurements of optically generated coherent spin packets, which are manipulated by  $E$  field pulses of  $E = 5.9 \frac{\text{mV}}{\mu\text{m}}$  and various pulse widths ranging from 0.5 to 8 ns. As expected, we observe spin precession for long field pulses of 8 ns. As the laser repetition time is 12 ns, this case is close to the dc Hanle limit as shown in Fig. 3. For shorter pulse widths,  $\theta_F$  always follows this spin precession curve during the field pulse. However, spin precession abruptly stops after the pulse has turned off after  $\delta w$ . This is seen by a simple exponential decay thereafter, which is observed for all pulse widths. In the TRFR curves, this is most clearly visible for pulse widths below 3 ns (orange curve) in Fig. 4a. We note that  $\theta_F$  changes sign for pulse widths  $\delta w$  at around 3 ns showing that the field pulse acts as  $\pi/2$  pulse, i.e. it coherently rotates the spin from the initial  $+z$  direction into the  $+x$  direction (see also Fig. 4c, center panel). For longer pulse widths ( $\delta w > 3$  ns),  $\theta_F$  becomes negative and reaches its minimum at about  $\delta w = 6$  ns. To further visualize this behavior, we plot  $\theta_F$  at a pump-probe delay of  $\Delta t = 8$  ns, for which the final spin direction is probed after coherent spin reorientation (see Fig. 4b). The minimum in  $\theta_F$  furthermore shows that the internal field pulse of 6 ns operates as  $\pi$  pulse, which rotates the spins by  $180^\circ$  from the  $+z$  into the  $-z$  direction (see also Fig. 4c, right panel). During spin reorientation,  $\theta_F$  significantly decreases from 0.09 mrad at  $\delta w = 0$  to -0.04 mrad at  $\delta w = 6$  ns. This decrease is caused by a partial spin dephasing of the coherent spin packet when the electric field pulse is applied (see also Fig. 3c). We can model the pulse width dependence of  $\theta_F$  by fitting  $T_2^*$  values from the TRFR data in Fig. 4a during the electric field pulse and thereafter. The resulting  $\theta_F$  is given by the green line in Fig. 4b for  $T_2^*(E = 0 \frac{\text{mV}}{\mu\text{m}}) = 3.8$  ns and  $T_2^*(E = 5.9 \frac{\text{mV}}{\mu\text{m}}) = 2.6$  ns, which is in good agreement with the  $T_2^*$  values in Fig. 3c. As discussed in Fig. 3d, reversing the electric field polarity will reverse the internal magnetic field direction. For negative electric field pulses, the resulting internal magnetic field pulse is thus oriented along the  $-y$  direction. For that case, coherent spin reorientation will occur in a clockwise direction, i.e. towards the  $-x$  direction. Using bipolar electric field pulses we therefore achieve full 2D coherent control over the final spin direction.



In conclusion, we have demonstrated to achieve full time-resolved electrical phase control of electron spin packet orientation within a 2D plane in InGaAs without the application of external magnetic fields. Some of us have shown recently that linearly polarized light can be utilized to achieve full 2D control of the initial spin direction [31]. Adding the electric field driven spin rotation to this new technique, we expect being able to achieve full 3D control of the spin orientation, which could provide an important step toward all-electrical spintronics without ferromagnets.

This work was supported by DFG through FOR 912.

---

\* e-mail: bernd.beschoten@physik.rwth-aachen.de

- [1] Y. Ohno *et al.*, Nature (London) **402**, 790 (1999).
- [2] S. A. Crooker *et al.*, Science **309**, 2191 (2005).
- [3] G. Kioseoglou *et al.*, Nature Materials **3**, 799 (2004).
- [4] X. Lou *et al.*, Nat. Phys **3**, 197 (2007).
- [5] D. Awschalom and N. Samarth, Physics **2**, 50 (2009).
- [6] J.E. Hirsch, Phys. Rev. Lett. **83**, 1834 (1999).
- [7] S. Zhang, Phys. Rev. Lett. **85**, 393 (2000).
- [8] Y. Kato *et al.*, Nature (London) **306**, 1910 (2004).
- [9] J. Wunderlich *et al.*, Phys. Rev. Lett. **94**, 047204 (2005).
- [10] V. Sih *et al.*, Nat. Phys. **1**, 31 (2005).
- [11] E. S. Garlid *et al.*, Phys. Rev. Lett. **105**, 156602 (2010).
- [12] V. M. Edelstein, Solid State Commun. **73**, 233 (1990).
- [13] Y. K. Kato *et al.*, Phys. Rev. Lett. **93**, 176601 (2004).
- [14] N. P. Stern *et al.*, Phys. Rev. Lett. **97**, 126603 (2006).
- [15] W. Koehl *et al.*, Appl. Phys. Lett. **95**, 072110 (2009).
- [16] A. G. Aronov and Y. B. Lyanda-Geller, Sov. JETP Lett. **50**, 431 (1989).
- [17] H.-A. Engel, E. I. Rashba, and B. I. Halperin, Phys. Rev. Lett. **98**, 036602 (2007).
- [18] M.-H. Liu, S.-H. Chen, and C.-R. Chang, Phys. Rev. B **78**, 165316 (2008).
- [19] B. Das *et al.*, Phys. Rev. B **39**, 1411 (1989).
- [20] G. Engels *et al.*, Phys. Rev. B **55**, R1958 (1997).

- [21] T. Koga *et al.*, Phys. Rev. Lett. **89**, 046801 (2002).
- [22] S. D. Ganichev *et al.*, Phys. Rev. Lett. **92**, 256601 (2004).
- [23] L. Meier *et al.*, Nat. Phys. **3**, 650 (2007).
- [24] B. M. Norman *et al.*, Phys. Rev. B **82**, 081304 (2010).
- [25] J. Nitta *et al.*, Phys. Rev. Lett. **78**, 1335 (1997).
- [26] S. Gosh *et al.*, Appl. Phys. Lett. **92**, 162109 (2008).
- [27] Y. Kato *et al.*, Nature (London) **427**, 50 (2004).
- [28] R. I. Dzhioev *et al.*, Phys. Rev. B **66**, 245204 (2002).
- [29] J. M. Kikkawa and D. D. Awschalom, Phys. Rev. Lett. **80**, 4313 (1998).
- [30] See supplemental material for detailed descriptions.
- [31] K. Schmalbuch *et al.*, Phys. Rev. Lett. **105**, 246603 (2010).